# Predicting the optimal geometry of microneedles and their array for dermal vaccination using a computational model

Anne M. Römgens[a], Dan L. Bader[a,b], Joke A. Bouwstra[c], Cees W.J. Oomens[a]

[a]*Soft Tissue Biomechanics and Engineering, Department of Biomedical Engineering, Eindhoven University of Technology, P.O. Box 513, 5600 MB Eindhoven, the Netherlands.*

[b]*Faculty of Health Sciences, University of Southampton, Southampton SO17 1BJ, UK.*

[c]*Division of Drug Delivery Technology, Leiden Academic Centre for Drug Research, Leiden University, P.O. Box 9502, 2300 RA Leiden, the Netherlands.*

Corresponding author: A.M. Römgens, Soft Tissue Biomechanics and Engineering, Department of Biomedical Engineering, Eindhoven University of Technology, PO Box 513, 5600 MB Eindhoven, The Netherlands. Tel.: +31402475415, E-mail address: a.m.romgens@tue.nl

## Abstract

Microneedle arrays have been developed to deliver a range of biomolecules including vaccines into the skin. These microneedles have been designed with a wide range of geometries and arrangements within an array. However, little is known about the effect of the geometry on the potency of the induced immune response. The aim of this study was to develop a computational model to predict the optimal design of the microneedles and their arrangement within an array. The three-dimensional finite element model described the diffusion and kinetics in the skin following antigen delivery with a microneedle array. The results revealed an optimum distance between microneedles based on the number of activated antigen presenting cells, which was assumed to be related to the induced immune response. This optimum depends on the delivered dose. In addition, the microneedle length affects the number of cells that will be involved in either the epidermis or dermis. By contrast, the radius at the base of the microneedle and release rate only minimally influenced the number of cells that were activated. The model revealed the importance of various geometric parameters to enhance the induced immune response. The model can be developed further to determine the optimal design of an array by adjusting its various parameters to a specific situation.

**Keywords:** finite element model; vaccine delivery; microneedles; pharmacokinetic model; antigen kinetics;

## 1. Introduction

Vaccines are currently delivered into the muscle or subcutaneous tissues with a hypodermic needle and syringe. However, the skin is rich in immune responsive cells and is, therefore, a potential location for the delivery of a vaccine. Vaccine administration into the skin can be beneficial in terms of pain sensation, efficiency, and safety. To deliver vaccines into the viable layers of the skin, microneedle arrays are being developed. These arrays contain small projections, the microneedles, which are arranged on a back plate. Depending on the delivery approach, the microneedle can be in different forms, including hollow, coated or dissolvable microneedles (van der Maaden et al. 2012; Kim et al. 2012). In recent years, these microneedles have been designed with a wide variety of geometries. The influence of the geometry on their penetration properties has been recently examined (Donnelly et al. 2010; Crichton et al. 2011; Römgens et al. 2014). However, little is known about the influence of this geometry and the microneedle arrangement within an array on the potency of the induced immune response; how the geometry influences the distribution of antigens in the skin, or the binding and internalization by cells, and the subsequent activation of antigen presenting cells (APCs) residing in the skin.

One study using coated microneedles indicated that the immune response was slightly increased when ovalbumin was applied to a larger skin area, but generally independent of microneedle length and density (Widera et al. 2006). By contrast, an optimum density was suggested in another study using coated microneedles (Depelsenaire et al. 2014). In addition, the total microneedle volume (Carey et al. 2011; Pearson et al. 2015) and the surface area of application (van der Maaden et al. 2014) were reported to influence the immune response when an antigen was topically applied before or after microneedle treatment. These previous studies suggest that the geometry of the array and its microneedles can be optimized to increase the potency of the induced immune response.

Computational and analytical models have previously been used to describe drug delivery by

microneedles (Lv et al. 2006; Al-Qallaf, Das, et al. 2009; Al-Qallaf, Mori, et al. 2009; Zhang et al. 2009; Olatunji et al. 2012; Kim et al. 2015), with particular focus on the delivery of the drug to the blood circulation. In addition, a model has been recently developed to predict the dissolution of a microneedle and the resulting drug concentration in the skin as function of time (Kim et al. 2015). However, these models do not focus on the kinetics in the skin and can, therefore, not be used to predict the internalization of antigens in the cells and the subsequent activation of cells, which is an essential step in evoking an immune response.

The aim of the current study was to develop a finite element model that was able to predict the optimal geometry of microneedles and their arrangement within an array for the purpose of vaccine delivery. This model was designed to predict the spatial-temporal diffusion of antigens released from a coated microneedle, and includes skin kinetics, as described in our previously developed compartment model (Römgens et al. 2016). The efficiency of the design was determined by means of the number of antigen presenting cells that were activated.

## 2. Methods

### *2.1 Model geometry*

A microneedle array was assumed to consist of a number of conically shaped microneedles placed in a regular grid with a centre-to-centre distance or spacing, $S$. Due to symmetry of the microneedle and array, a quarter of a microneedle within a rectangular skin sample could be used as a representative volume element (RVE). Hence, combining multiple RVEs will result in a microneedle array ignoring the effect of microneedles at the edge of the array. The geometry of the microneedle itself could be described by its length, $l_{MN}$, and radius at the base, $r_b$ (Figure 1). Coated microneedles were considered and modelled with a coating layer thickness, $t_c$, of 0.02 mm around the microneedle. The skin was divided into two layers, namely, the epidermis with a thickness, $t_e$, of 0.2 mm and the dermis with a thickness, $t_d$, of 1.8 mm. The default parametric

values describing the microneedle geometry and spacing within the array are summarized in Table 1.

The model was implemented in a finite element package, Abaqus (v6.14-1, Dassault Systèmes Simulia Corp., Providence, RI, USA). The mesh contained linear tetrahedral elements (DC3D4) with a fine mesh around the microneedle and increasing coarseness towards the edges of the model (Figure 1b and c).

### *2.2 Transport and kinetics in the skin*

After a microneedle array penetrated into the skin, the antigen coating of the microneedles will start to release antigens, which will diffuse into the skin. The cells residing in the skin bind and internalize these antigens via receptor-mediated endocytosis, which was assumed to occur in all available cells. The two populations of antigen presenting cells, the Langerhans cells in the epidermis and the dermal dendritic cells in the dermis, mature and start to migrate towards the lymph nodes upon antigen uptake. In addition to internalization, antigens can be taken up into the blood and lymph capillaries located in the dermis and deeper tissue layers.

This process of antigen release, diffusion, and internalization by the cells can be described by a set of partial differential equations (1)-(6) (Römgens et al. 2016):

$$\frac{\partial C_{MN}}{\partial t} = \nabla(D_{MN}\nabla C_{MN}), \tag{1}$$

$$\frac{\partial C_{ECM,e}}{\partial t} = \nabla\left(D_e\nabla C_{ECM,e}\right) - k_a C_{ECM,e}\left(R_{tot,e} - C_{rec} - C_{cells}\right) + k_d C_{rec}, \tag{2}$$

$$\frac{\partial C_{ECM,d}}{\partial t} = \nabla\left(D_d\nabla C_{ECM,d}\right) - k_a C_{ECM,d}\left(R_{tot,d} - C_{rec} - C_{cells}\right) + k_d C_{rec} - k_c C_{ECM,d}, \tag{3}$$

$$\frac{\partial C_{rec}}{\partial t} = k_a C_{ECM,i}\left(R_{tot,i} - C_{rec} - C_{cells}\right) - (k_d + k_{int})C_{rec}, \tag{4}$$

$$\frac{\partial C_{circ}}{\partial t} = k_c C_{ECM,d}, \tag{5}$$

$$\frac{\partial C_{cells}}{\partial t} = k_{int} C_{rec}, \tag{6}$$

where $C_{MN}$ is the antigen concentration in the coating of the microneedle, $C_{ECM,i}$ the antigen concentration in the extracellular matrix (ECM) with $i = e$ and $d$ for the epidermis and dermis, $C_{rec}$

the concentration of antigens bound to receptors, $C_{cells}$ the antigen concentration taken up by the cells, and $C_{circ}$ the antigen concentration taken up by the microcirculation (both lymph and blood). These concentrations are all a function of the $x$-, $y$-, and $z$-coordinates and time $t$. $R_{tot,i}$ is the initial receptor concentration and $D_j$ the diffusion coefficient with $j = MN$, $e$, and $d$, representing the coating of the microneedle, epidermis, and dermis, respectively. The velocity of the various processes involved were prescribed with rate constants $k_\beta$ with $\beta = a$, $d$, $int$, and $c$. These represent the association and dissociation rate of the antigen-receptor binding, the rate of internalization of the antigen-receptor complex and the rate of uptake into the circulation, respectively.

The skin kinetics was implemented in the finite element model using the subroutine *hetval*, in which the change in concentration was calculated at each integration point for every increment. This was achieved in an explicit manner using (1)-(6).

The parameter values that were used to describe the kinetics were based on average values from the literature and are summarized in Table 2. Our previous study revealed that the rate constants had little effect on the output of the model and can therefore be taken from general values from the literature (Römgens et al. 2016). The initial receptor concentration was estimated from the cell density (6.2 x $10^4$ cells/mm$^3$ for the dermis, 1.3 x $10^6$ cells/mm$^3$ for the epidermis) and the number of receptors per cell (1 x $10^5$) for both the epidermis and dermis (Avraméas et al. 1996; McLellan et al. 1998; Szolnoky et al. 2001; Mulholland et al. 2006; Römgens et al. 2016). The diffusion coefficient in both these layers was based on measurements with 40 kDa dextran (Römgens et al. 2015).

### *2.3 Initial and boundary conditions*

In the initial state of the model, the concentration of the coating of the microneedle was $C_{MN,0}$, whereas all other concentrations were zero. This initial coating concentration was obtained by

dividing the delivery dose per microneedle $d_{MN}$ by the volume of the coating. The default dose per microneedle was 5.2 x $10^{-8}$ µmol, unless stated otherwise, and was based on a total delivery dose of 0.3 µg diphtheria toxoid to be delivered by an array containing 100 microneedles.

During the simulation, the concentration of the ECM was prescribed to be zero in the plane $ABCD$ of the skin (Figure 1a). This represented the transport away from the skin due to larger blood and lymph vessels. The side edges were impermeable to antigens, simulating the symmetry to the adjacent skin, in which the concentration at the edge would be the same. In addition, the top plane was also impermeable to simulate the stratum corneum.

The model ran until steady state was attained, when the change in the ECM and microneedle concentration ((1)-(3)) was less than 1 x $10^{-15}$ µmol/s.

### *2.4 Model variations: optimization of array design*

Specific geometric parameters were varied to determine their influence on the efficiency of evoking an immune response. These included the distance, $S$, between the centres of two adjacent microneedles in an array, the length of the microneedle, $l_{MN}$, and the radius at the base, $r_b$. In addition, the dose delivered by the microneedle, $d_{MN}$, and the time of release from the microneedle were varied, the latter parameter of which was controlled by the diffusion coefficient of the coating layer.

The efficiency of the immune response was determined by two factors:

- The proportion of the total number of antigens taken up by the cells.
- The number of activated antigen presenting cells in the epidermis and dermis.

The activation of antigen presenting cells to start maturing and migrating towards the lymph nodes was assumed to depend on their level of saturation, $L_{sat}$. This was defined as the ratio between the concentration internalized by the cells and its theoretical maximum. The latter was equal to the initial receptor concentration, $R_{tot,i}$, of the specific skin layer, resulting in the following equation:

$$L_{sat} = C_{cells,ss}/R_{tot,i}\ , \qquad (7)$$

where $C_{cell,ss}$ is the antigen concentration taken up by the cells in steady state. This level of saturation was dependent on the $x$-, $y$-, and $z$-coordinates. If the saturation threshold, $\theta$, was exceeded, then the antigen presenting cells were assumed to be activated. The number of activated antigen presenting cells was subsequently determined based on the total cell density in the epidermis and dermis, and the assumption that the antigen presenting cells represent 10% of the total cell population taking up antigens.

## 3 Results

### *3.1 Distribution with default microneedle*

The progression of the antigen concentration within the extracellular matrix and the saturation of the cells within this matrix for the default microneedle geometry are presented in Figure 2. The initial high antigen concentration of the microneedle decreases while the antigens diffuse into the extracellular matrix. Simultaneously, the antigens bind and are taken up by the cells, increasing the level of saturation of the cells up to its maximal level. At steady state, the antigen concentration in the extracellular matrix is approximately zero. In addition, a large portion of the cells in the epidermis and dermis are close to full saturation in this simulation with the default features of the microneedle geometry.

### *3.2 Effect of spacing between microneedles*

The distance between the microneedles was varied between 0.25 and 4 mm, while the other parameters retained their default values (Tables 1 and 2). An optimum distance was revealed with respect to the number of APCs that were activated (Figure 3), which was dependent on the saturation threshold, $\theta$, at which the cells were activated. Moreover, the maximum number of activated APCs occurred at a different microneedle spacing for the dermis and epidermis (Figure 3b and c). For example, at a saturation threshold of 0.5, the maximum number of activated cells

occurred at a spacing of approximately 1 mm, which was also the optimal distance for activating the cells in the epidermis. However, for the dermis its optimum occurred at a distance of 1.5 mm. Below the optimal distance the activation of cells rapidly decreased. By contrast, above the optimal distance, the number of activated cells reached a constant value just below its maximum.

At a spacing below 1 mm, the proportion of the total number of antigens taken up by the cells rapidly decreased (Figure 4). Therefore, at lower values of the spacing more antigens were transported to the circulation, which may result in dissipation of antigens.

The optimum value for the spacing for cell activation and, thus, the value below which a larger part of the antigens end up in the circulation were dependent on the dose administrated with a single microneedle. At a lower dose, the optimal spacing decreased (data not shown).

### *3.3 Effect of microneedle length*

The length of the microneedle was varied between 0.05 and 1.45 mm, while retaining the default values of the other parameters. The total number of activated APCs decreased with increasing microneedle length, as did the activation of cells in the epidermis (Figure 5a and b). By contrast, in the dermis more cells were activated with an increase in the microneedle length (Figure 5c). Hence, the ratio between the number of activated antigen presenting cells in the epidermis and dermis decreased with increasing microneedle length. At a saturation level of 1, this ratio decreased maximally from 27.9 for a 0.05 mm long microneedle to 1.5 for a length of 1.45 mm. However, at a saturation level of 0.1, the corresponding ratios were 7.4 and 5.7, respectively.

The increase in the number of activated cells in the dermis was observed up to a length where all cells were activated. This occurred, for example, at a saturation threshold of 0.1 and a length above 0.9 mm (Figure 5c). At a larger distance between the microneedles this maximum was not yet reached in the dermis at a length of 1.45 mm (data not shown). In addition, there was a small linear decrease in the proportion of antigens taken up by the cells from 97% to 92% over the range of microneedle lengths examined.

### *3.4 Effect of microneedle base radius*

The radius at the base of the microneedle was varied between 0.0875 and 0.26 mm, while maintaining the default values of the other parameters. Similar to the length of the microneedle, the radius of the microneedle generally determined the location at which the antigens were delivered. The number of activated APCs varied slightly with the radius of the microneedle, as indicated in Figure 6. In the epidermis, the number increased at a high saturation threshold (Figure 6b), reflecting the reduced distance between the outside of two adjacent microneedles and tending towards the optimal distance (Figure 3). At lower saturation thresholds, all available cells were activated. However, the number of activated cells decreased with increasing radius (Figure 6b). This effect was caused by the corresponding increase in microneedle volume, reducing the skin volume and thereby the available cells. This effect will not occur in an experimental setup. By contrast, in the dermis the number of activated cells was independent of the radius, except at the high saturation threshold (Figure 6c). When the spacing of the microneedles was significantly higher than the optimal spacing, the radius did not have any effect on the number of activated cells (data not shown).

The radius of the microneedle did not have any effect on the fraction of antigen taken up by the cells and the fraction released to the circulation.

### *3.5 Effect of delivered dose*

To assess the effect of the delivered dose, the dose was varied two orders of magnitude from $5.2 \times 10^{-9}$ to $5.2 \times 10^{-7}$ µmol, while maintaining the default values of the other parameters. The delivered dose clearly affected the activation of cells (Figure 7). The saturation of the cells increased with the delivered dose up to full saturation levels, beyond which any increase in dose was released into the circulation.

### *3.6 Effect of release time*

The time of release of the coating from the microneedle did not have any effect on the activation of cells (Figure 8) or the proportion of the antigens that was taken up by the circulation.

## 4 Discussion

The developed model, which described the spatial temporal diffusion of antigens and their kinetics in the skin after delivery with a microneedle array, was used to predict the number of activated antigen presenting cells and the proportion of antigens internalized by the cells. In particular, the effect of the microneedle and array geometry on the distribution and activation of cells was assessed. Assuming the number of activated cells was directly related to the induced immune response, the optimal geometry could be predicted. The simulations revealed an optimum for the centre-to-centre distance of the microneedles. The total number of activated cells decreased with microneedle length, although there was a corresponding increase in the number activated in the dermis. In addition, the applied dose significantly affected the number of activated cells. By contrast, the effect of the radius of the microneedle was only apparent when the spacing was close to its optimum. Changing the release rate of the antigens from the microneedle did not have any effect. In general, the percentage of the total number of antigens internalized by the cells was high, but could rapidly decrease in situations where all cells were saturated.

The synergistic effect of adjacent microneedles can explain the optimal distance between microneedles. At a spacing significantly larger than the optimum, the antigens released from a microneedle will not reach the same location as those released from other microneedles (Figure 9a). Hence, further increasing the spacing, does not affect the activation of cells. At the optimal distance, the antigens from multiple microneedles can contribute to the activation of the cells located between the microneedles (Figure 9b). However, at a further decrease in spacing, the influential zone of the microneedles will overlap excessively, resulting in the dissipation of antigens (Figure 9c). As a result, the optimal spacing is dependent on the dose delivered by a single microneedle and the available binding sites for the antigens. Therefore, at a certain predetermined

dose per microneedle, the array geometry can be adjusted to generate the highest level of activated antigen presenting cells. Assuming the number of these activated cells is directly related to the potency of the immune response, the simulations confirm previous experimental observations in which the evoked immune response was dependent on the area to which the antigens were exposed (Widera et al. 2006; van der Maaden et al. 2014), as a larger spacing in the model implied a larger application area. It is interesting to note that Widera and coworkers (Widera et al. 2006) reported no such effect when the density alone was changed. However, for a fixed dose, the model simulations predict that it is largely dependent on the densities examined if it will affect the number of activated cells, and thereby the potency of the immune response. In one study, an optimal microneedle distance was reported (Depelsenaire et al. 2014), although the authors attributed this effect to the colocalization of antigen delivery with signals from dead cells. Indeed, these signals, resulting from microneedle insertion, may influence the immune response.

The different subsets of antigen presenting cells can induce a different immune response. The simulations revealed that the length of the microneedle, and thus the location at which the antigens were delivered affects the ratio of cells activated in the epidermis and dermis. Hence, the length may be adapted to target either Langerhans cells in the epidermis or dermal dendritic cells residing in the dermis. However, a previous study reported that the immune response was mostly independent of the microneedle length (Widera et al. 2006). Nevertheless, when a relatively high dose was used, the effect of length may have been masked due to the complete saturation of all cells. Moreover, the model showed that more antigens were taken up into blood and lymphatic circulation at either increased microneedle lengths or a higher dose. The antigens taken up in the lymph vessels can transport to the lymph nodes and activate lymph node resident dendritic cells (Ueno et al. 2007) and thereby contribute to the initiation of an immune response. This potential mechanism was not considered in the present model. Indeed, large molecules are generally taken up in the lymphatics as opposed to the blood circulation (Ibrahim et al. 2012).

The model may be further extended by including signalling molecules and cell migration. Currently, a homogeneous cell density was considered and fixed within each layer. However, migration of cells can occur, initiated by the release of molecules, such as cytokines and chemokines, from skin cells (Ueno et al. 2007; Koutsonanos et al. 2013). These molecules provide a signal to cells from both inside and outside the skin to migrate towards the location of secretion (Del Pilar Martin et al. 2012; Koutsonanos et al. 2013) and thereby repopulating the skin and changing the number and distribution of cells within the skin. In addition, these signalling molecules can influence the maturation and migration of antigen presenting cells towards the lymph nodes (Koutsonanos et al. 2013). If these processes were included in the model, the release rate may prove to influence the evoked immune response when a sustained period is simulated, since it has been reported that a vaccination regime over many days can increase the response (Johansen et al. 2008). However, with the present static cell density, no long term processes could be predicted and, as a result, the release rate did not have any influence on cell activation. The current model varies the release rate by adapting the diffusion coefficient in the coating layer. The release rate may also be varied by changing the coating thickness. Applying the same dose with a thinner coating layer will increase the concentration of the coating and therefore the release rate. Although, the current coating thickness of 0.02 mm may be considered high, it should not influence the results as the release rate did not influence the steady state in the model (Figure 8). The model could also be refined by incorporating the partitioning between the different layers in the skin.

Using the present model, the effect of various parameters was determined on the number of activated cells in both the epidermis and dermis. However, the absolute values for geometry parameters should not be interpreted as the optimal values. For each specific situation, the relevant kinetic parameters, number of receptors and dose should be determined. In our previous study, we showed that from these parameters the number of receptors and dose had the largest influence on the output of the model (Römgens et al. 2016). In the current study, the model was used to provide

an insight into the efficiency of dermal vaccination, however, the same approach can be adopted for the application of other drugs or for transdermal delivery.

In conclusion, the developed model can be used to optimize the geometry of microneedles and their array to increase activation of antigen presenting cells and subsequently the potency of the immune response. It revealed that there exists an optimum distance between the microneedles within the array, which was dependent on the applied dose and may be different when targeting the epidermis or the dermis. In addition, the length of the microneedle influenced the ratio of cells activated in both skin layers. By contrast, the radius at the base of the microneedle and the release rate produced only minimal effects on the resulting the activation of targeted cells.

**Acknowledgements**

We thank the Tyndall National Institute, Cork, Ireland for supplying microneedle arrays. This research is supported by the Dutch Technology Foundation STW, which is part of the Netherlands Organisation for Scientific Research (NWO), and which is partly funded by the Ministry of Economic Affairs (Project no. 11259).

**References**

Al-Qallaf B, Das DB, Davidson A. 2009. Transdermal drug delivery by coated microneedles: geometry effects on drug concentration in blood. Asia-Pac J Chem Eng. 4:845–857.

Al-Qallaf B, Mori D, Olatunji L, Das DB, Cui Z. 2009. Transdermal drug delivery by microneedles: does skin metabolism matter? Int J Chem React Eng. 7:A69.

Avraméas A, McIlroy D, Hosmalin A, Autran B, Debré P, Monsigny M, Roche AC, Midoux P. 1996. Expression of a mannose/fucose membrane lectin on human dendritic cells. Eur J Immunol. 26:394–400.

Carey JB, Pearson FE, Vrdoljak A, McGrath MG, Crean AM, Walsh PT, Doody T, O'Mahony C, Hill AVS, Moore AC. 2011. Microneedle array design determines the induction of protective memory CD8+ T cell responses induced by a recombinant live malaria vaccine in mice. PloS One. 6:e22442.

Crichton ML, Donose BC, Chen X, Raphael AP, Huang H, Kendall MAF. 2011. The viscoelastic, hyperelastic and scale dependent behaviour of freshly excised individual skin layers. Biomaterials. 32:4670–4681.

Del Pilar Martin M, Weldon WC, Zarnitsyn VG, Koutsonanos DG, Akbari H, Skountzou I, Jacob J, Prausnitz MR, Compans RW. 2012. Local response to microneedle-based influenza immunization in the skin. mBio. 3:e00012–12.

Depelsenaire ACI, Meliga SC, McNeilly CL, Pearson FE, Coffey JW, Haigh OL, Flaim CJ, Frazer IH, Kendall MAF. 2014. Colocalization of cell death with antigen deposition in skin enhances vaccine immunogenicity. J Invest Dermatol. 134:2361–2370.

Donnelly RF, Garland MJ, Morrow DIJ, Migalska K, Singh TRR, Majithiya R, Woolfson AD. 2010. Optical coherence tomography is a valuable tool in the study of the effects of microneedle geometry on skin penetration characteristics and in-skin dissolution. J Controlled Release. 147:333–341.

Ibrahim R, Nitsche JM, Kasting GB. 2012. Dermal clearance model for epidermal bioavailability calculations. J Pharm Sci. 101:2094–2108.

Johansen P, Storni T, Rettig L, Qiu Z, Der-Sarkissian A, Smith KA, Manolova V, Lang KS, Senti G, Müllhaupt B, et al. 2008. Antigen kinetics determines immune reactivity. Proc Natl Acad Sci. 105:5189–5194.

Kim KS, Ita K, Simon L. 2015. Modelling of dissolving microneedles for transdermal drug delivery: theoretical and experimental aspects. Eur J Pharm Sci. 68:137–143.

Kim Y-C, Park J-H, Prausnitz MR. 2012. Microneedles for drug and vaccine delivery. Adv Drug Deliv Rev. 64:1547–1568.

Koutsonanos DG, Compans RW, Skountzou I. 2013. Targeting the skin for microneedle delivery of influenza vaccine. In: Katsikis PD, Schoenberger SP, Pulendran B, editors. Crossroads Innate Adapt Immun IV. Springer New York; p. 121–132.

Lv Y-G, Liu J, Gao Y-H, Xu B. 2006. Modeling of transdermal drug delivery with a microneedle array. J Micromechanics Microengineering. 16:2492–2501.

van der Maaden K, Jiskoot W, Bouwstra J. 2012. Microneedle technologies for (trans)dermal drug and vaccine delivery. J Controlled Release. 161:645–655.

van der Maaden K, Varypataki EM, Yu H, Romeijn S, Jiskoot W, Bouwstra J. 2014. Parameter optimization toward optimal microneedle-based dermal vaccination. Eur J Pharm Sci. 64:18–25.

McLellan AD, Heiser A, Sorg RV, Fearnley DB, Hart DNJ. 1998. Dermal dendritic cells associated with T lymphocytes in normal human skin display an activated phenotype. J Invest Dermatol. 111:841–849.

Metz B, Jiskoot W, Hennink WE, Crommelin DJA, Kersten GFA. 2003. Physicochemical and immunochemical techniques predict the quality of diphtheria toxoid vaccines. Vaccine. 22:156–167.

Mulholland WJ, Arbuthnott EAH, Bellhouse BJ, Cornhill JF, Austyn JM, Kendall MAF, Cui Z, Tirlapur UK. 2006. Multiphoton high-resolution 3D imaging of Langerhans cells and keratinocytes in the mouse skin model adopted for epidermal powdered immunization. J Invest Dermatol. 126:1541–1548.

Olatunji O, Das DB, Nassehi V. 2012. Modelling transdermal drug delivery using microneedles: effect of geometry on drug transport behaviour. J Pharm Sci. 101:164–175.

Pearson FE, O'Mahony C, Moore AC, Hill AVS. 2015. Induction of CD8+ T cell responses and protective efficacy following microneedle-mediated delivery of a live adenovirus-vectored malaria vaccine. Vaccine. 33:3248–3255.

Römgens AM, Bader DL, Bouwstra JA, Baaijens FPT, Oomens CWJ. 2014. Monitoring the penetration process of single microneedles with varying tip diameters. J Mech Behav Biomed Mater. 40:397–405.

Römgens AM, Bader DL, Bouwstra JA, Baaijens FPT, Oomens CWJ. 2015. Diffusion profile of macromolecules within and between human skin layers for (trans)dermal drug delivery. J Mech Behav Biomed Mater. 50:215–222.

Römgens AM, Bader DL, Bouwstra JA, Oomens CWJ. 2016. A theoretical compartment model for antigen kinetics in the skin. Eur J Pharm Sci. 84:18–25.

Szolnoky G, Bata-Csörgö Z, Kenderessy AS, Kiss M, Pivarcsi A, Novák Z, Nagy Newman K, Michel G, Ruzicka T, Maródi L, et al. 2001. A mannose-binding receptor is expressed on human keratinocytes and mediates killing of Candida albicans. J Invest Dermatol. 117:205–213.

Ueno H, Klechevsky E, Morita R, Aspord C, Cao T, Matsui T, Di Pucchio T, Connolly J, Fay JW, Pascual V, et al. 2007. Dendritic cell subsets in health and disease. Immunol Rev. 219:118–142.

Vainshtein I, Roskos LK, Cheng J, Sleeman MA, Wang B, Liang M. 2015. Quantitative measurement of the target-mediated internalization kinetics of biopharmaceuticals. Pharm Res. 32:286–299.

Widera G, Johnson J, Kim L, Libiran L, Nyam K, Daddona P, Cormier M. 2006. Effect of delivery parameters on immunization to ovalbumin following intracutaneous administration by a coated microneedle array patch system. Vaccine. 24:1653–1664.

Zhang R, Zhang P, Dalton C, Jullien GA. 2009. Modeling of drug delivery into tissues with a microneedle array using mixture theory. Biomech Model Mechanobiol. 9:77–86.

**Table 1 –** Default values to describe the microneedle geometry and their spacing within an array (Figure 1). These values were used unless stated otherwise.

| Parameter | Default value [mm] |
|---|---|
| $S$ | 1 |
| $l_{MN}$ | 0.3 |
| $r_b$ | 0.0875 |
| $t_e$ | 0.2 |
| $t_d$ | 1.8 |
| $t_c$ | 0.02 |

**Table 2 –** The default values for the rate constants, initial receptor concentrations, dose per microneedle, and diffusion coefficients are presented. These were based on values reported in the literature (Avraméas et al. 1996; McLellan et al. 1998; Szolnoky et al. 2001; Metz et al. 2003; Mulholland et al. 2006; Ibrahim et al. 2012; Vainshtein et al. 2015; Römgens et al. 2015). These values were used in all simulations unless stated otherwise.

| Parameter | Default value |
|---|---|
| $k_a$ | $1 \times 10^{5}$ $M^{-1}$ $s^{-1}$ |
| $k_d$ | $1 \times 10^{-3}$ $s^{-1}$ |
| $k_{int}$ | $1 \times 10^{-3}$ $s^{-1}$ |
| $k_c$ | $1 \times 10^{-5}$ $s^{-1}$ |
| $R_{tot,e}$ | $2.2 \times 10^{-7}$ µmol $mm^{-3}$ |
| $R_{tot,d}$ | $1.0 \times 10^{-8}$ µmol $mm^{-3}$ |
| $d_{MN}$ | $5.2 \times 10^{-8}$ µmol |
| $D_e$ | $8 \times 10^{-6}$ $mm^2$ $s^{-1}$ |
| $D_d$ | $21 \times 10^{-6}$ $mm^2$ $s^{-1}$ |
| $D_{MN}$ | $8 \times 10^{-6}$ $mm^2$ $s^{-1}$ |

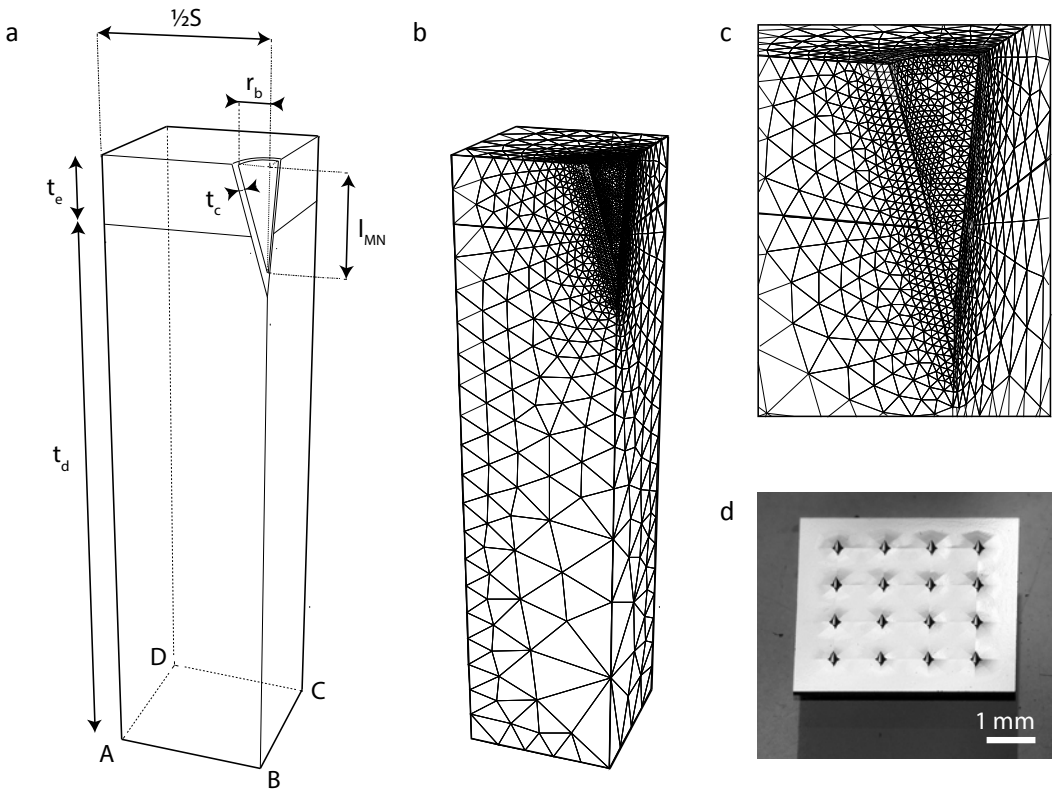


**Figure 1 –** Schematic representation of the microneedle and array geometry and the finite element mesh. (a) The microneedle was characterized by its length, $l_{MN}$, radius at the base, $r_b$, and coating thickness, $t_c$. The array can be described by the distance between the centres of two adjacent microneedles, $S$. The skin is divided in an epidermal and dermal layer with thicknesses $t_e$ and $t_d$, respectively. A single representative volume element is illustrated. (b) The mesh of the default microneedle (Table 1). (c) Close up of the mesh around the microneedle. (d) Example of a microneedle array from Tyndall National Institute, Cork, Ireland.

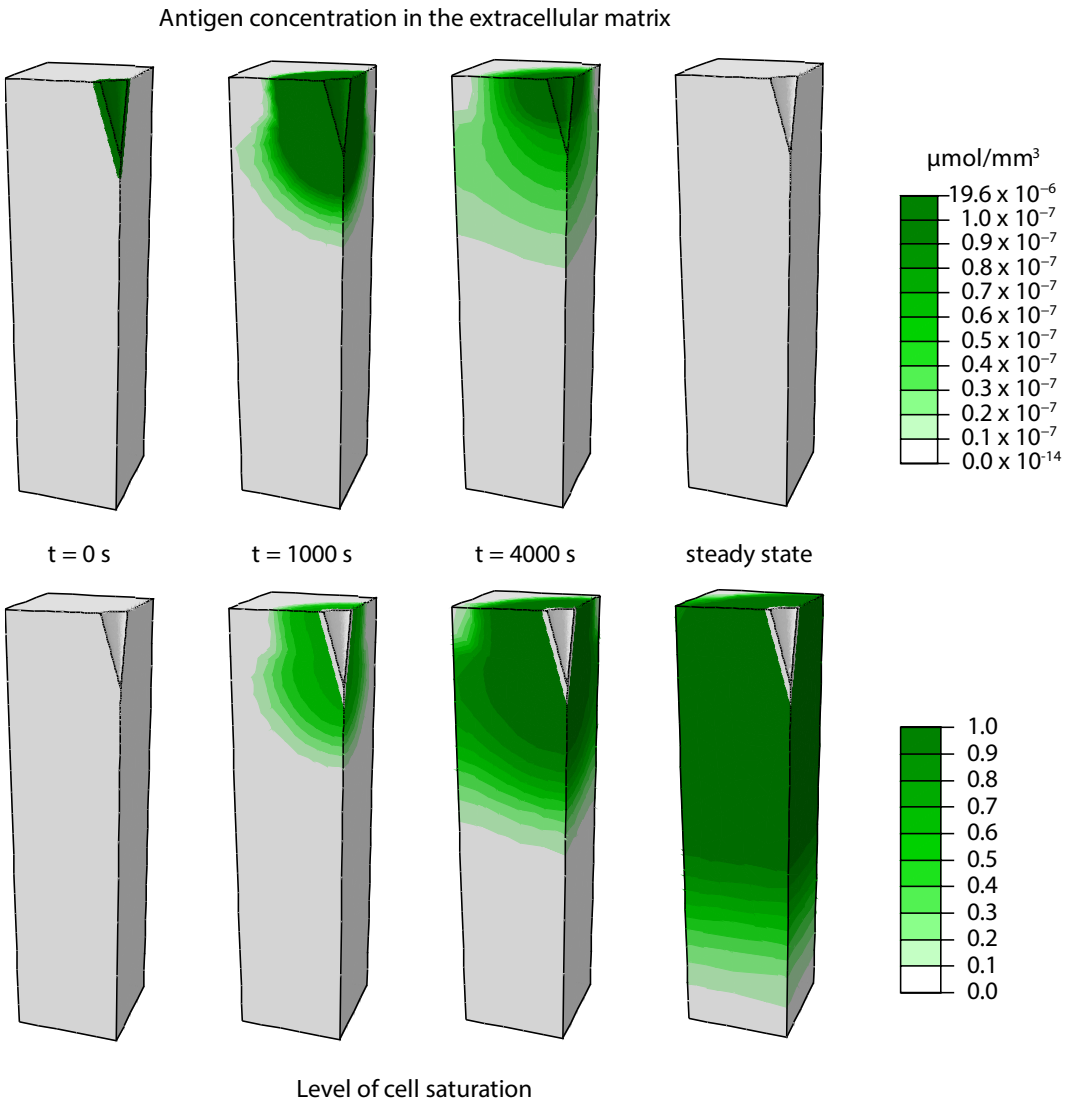


**Figure 2 –** The progress of antigen distribution within the extracellular matrix and the level of saturation of the cells simulated for the default microneedle geometry.

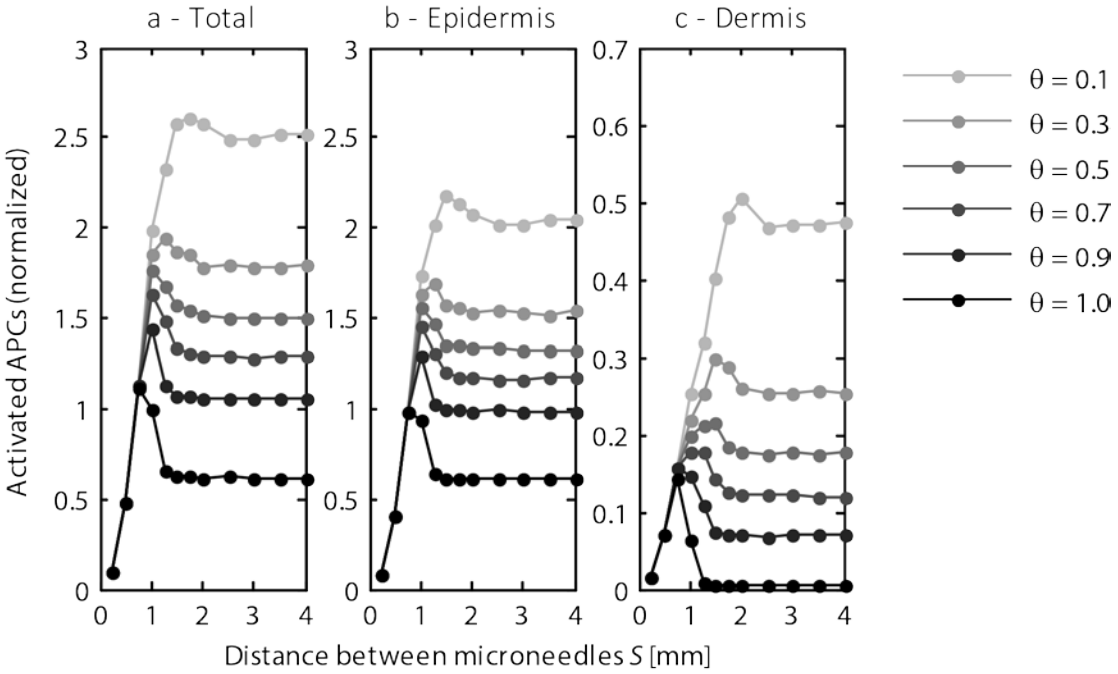


**Figure 3 –** The normalized number of activated APCs as a function of the distance between the microneedles within an array for the entire skin (a), the epidermis (b), and the dermis (c). All values were normalized to the total number of antigen presenting cells activated with the default microneedle geometry ($S$ = 1 mm) at a saturation threshold of 1. Each line represents a different saturation threshold, $\theta$. Note the different scale on the y-axis for the dermis.

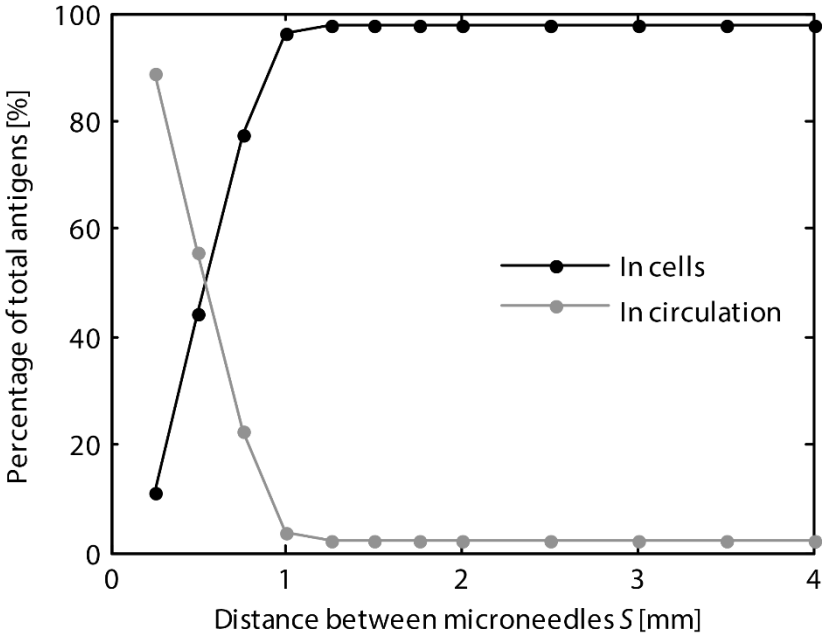


**Figure 4 –** Influence of the microneedle spacing on the percentage of the total number of antigens internalized by the cells and taken up into the circulation in steady state.

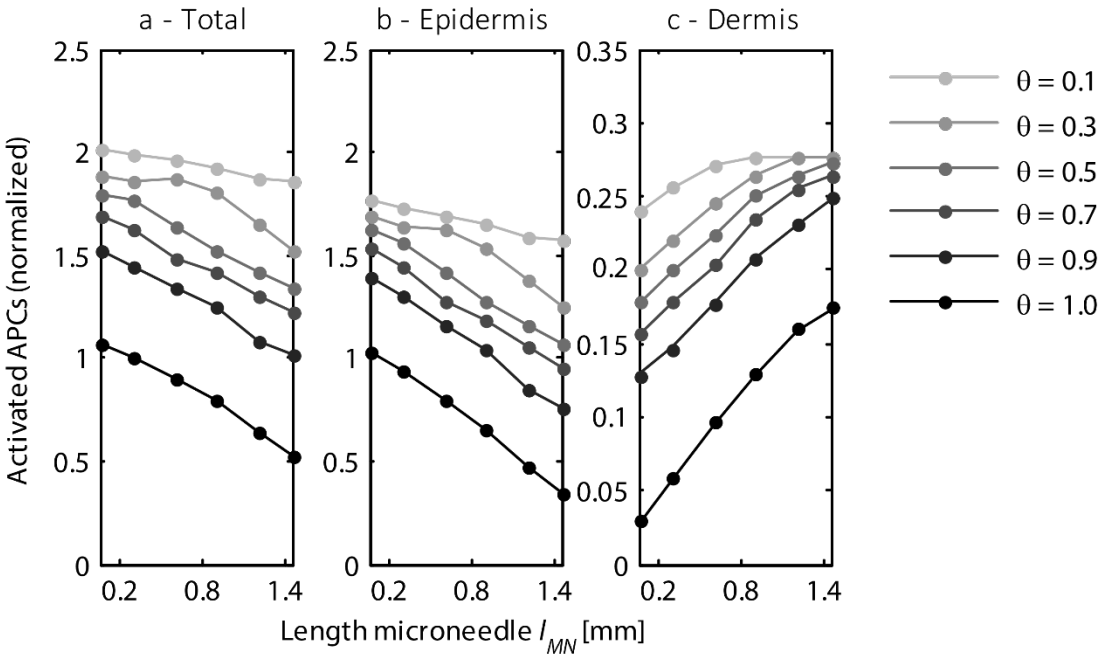


**Figure 5 –** The normalized number of activated APCs as a function of the length of the microneedle for the entire skin (a), the epidermis (b), and the dermis (c). All values were normalized to the total number of antigen presenting cells activated with the default microneedle geometry ($l_{MN}$ = 0.3 mm) at a saturation threshold of 1. Each line represents a different saturation threshold, $\theta$. Note the different scale on the y-axis for the dermis.

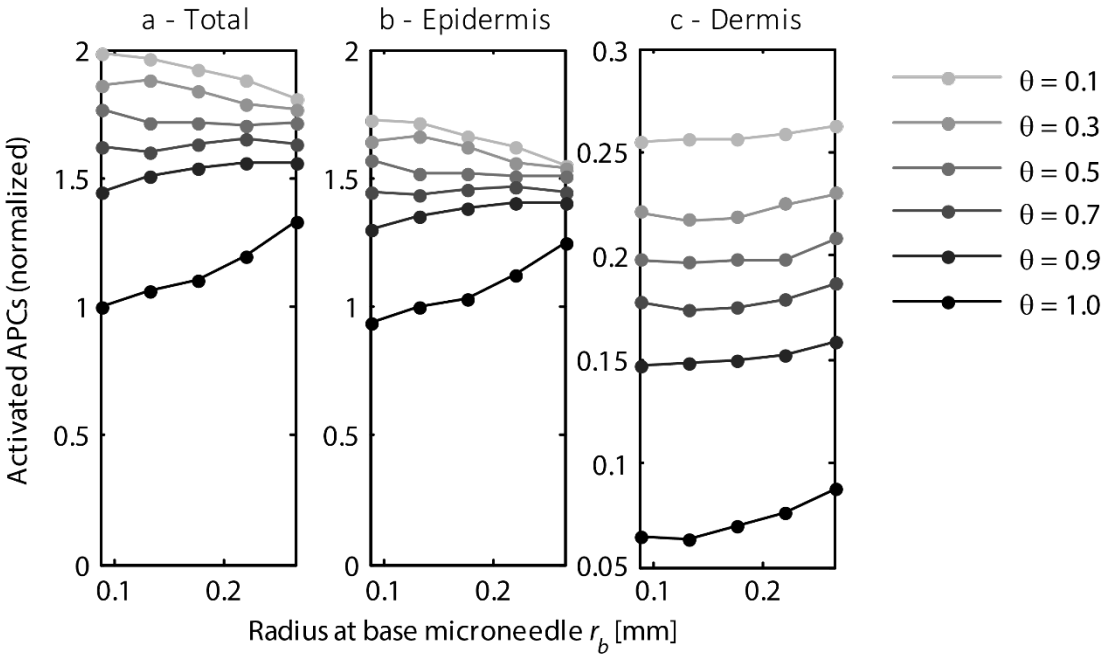


**Figure 6 –** The normalized number of activated APCs as a function of the radius of the microneedles at its base for the entire skin (a), the epidermis (b), and the dermis (c). All values were normalized to the total number of antigen presenting cells activated with the default microneedle geometry ($r_b$ = 0.0875 mm) at a saturation threshold of 1. Each line represents a different saturation threshold, $\theta$. Note the different scale on the y-axis for the dermis.

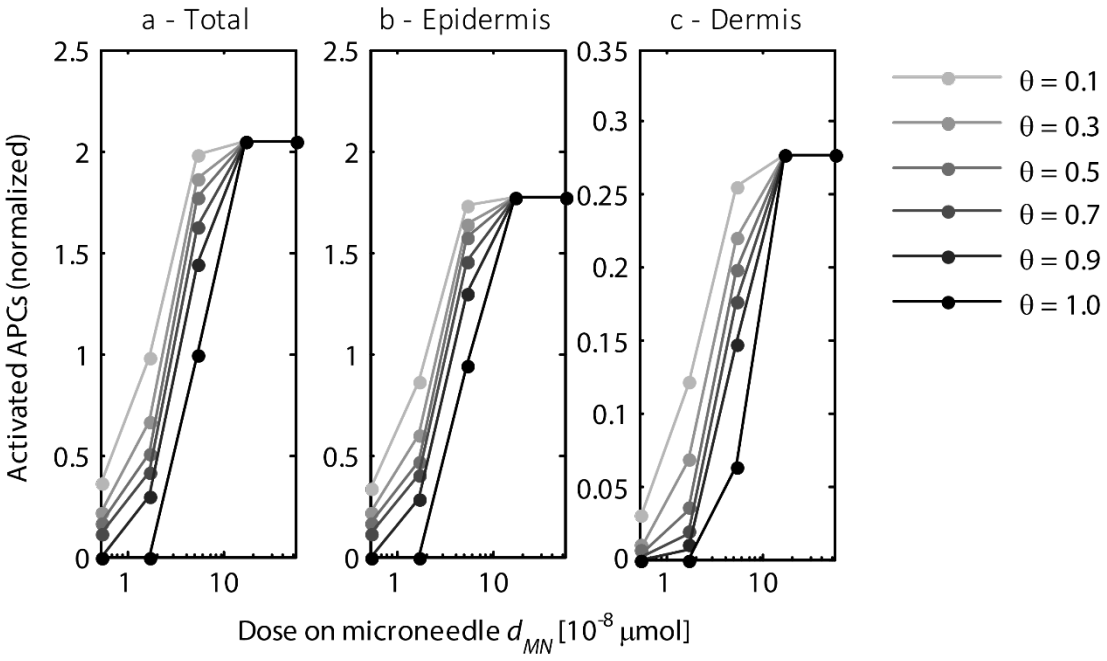


**Figure 7 –** The normalized number of activated APCs as a function of the delivered dose by a single microneedle for the entire skin (a), the epidermis (b), and the dermis (c). All values were normalized to the total number of antigen presenting cells activated with the default dose ($d_{MN}$ = 5.2 x $10^{-8}$ µmol) at a saturation threshold of 1. Each line represents a different saturation threshold, $\theta$. Note the logarithmic scale on the x-axis and the different scale on the y-axis for the dermis.

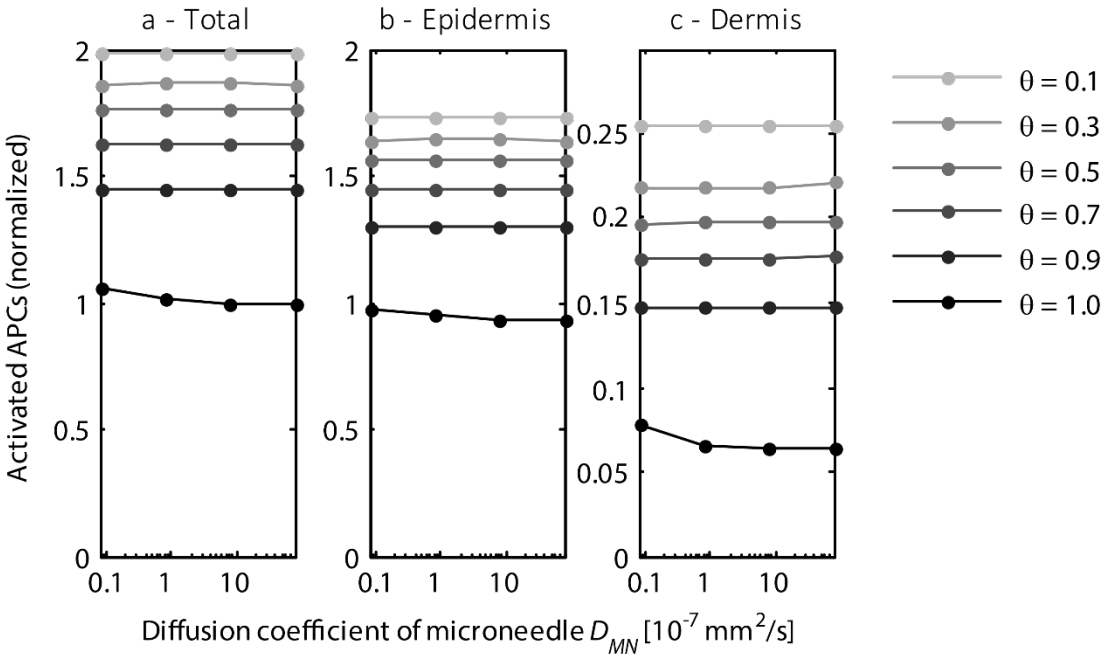


**Figure 8 –** The normalized number of activated APCs as a function of the delivered dose by a single microneedle for the entire skin (a), the epidermis (b), and the dermis (c). All values were normalized to the total number of antigen presenting cells activated with the default diffusion coefficient ($D_{MN}$ = 8 x $10^{-6}$ mm$^2$ s$^{-1}$) at a saturation threshold of 1. Each line represents a different saturation threshold, $\theta$. Note the logarithmic scale on the x-axis and the different scale on the y-axis for the dermis.

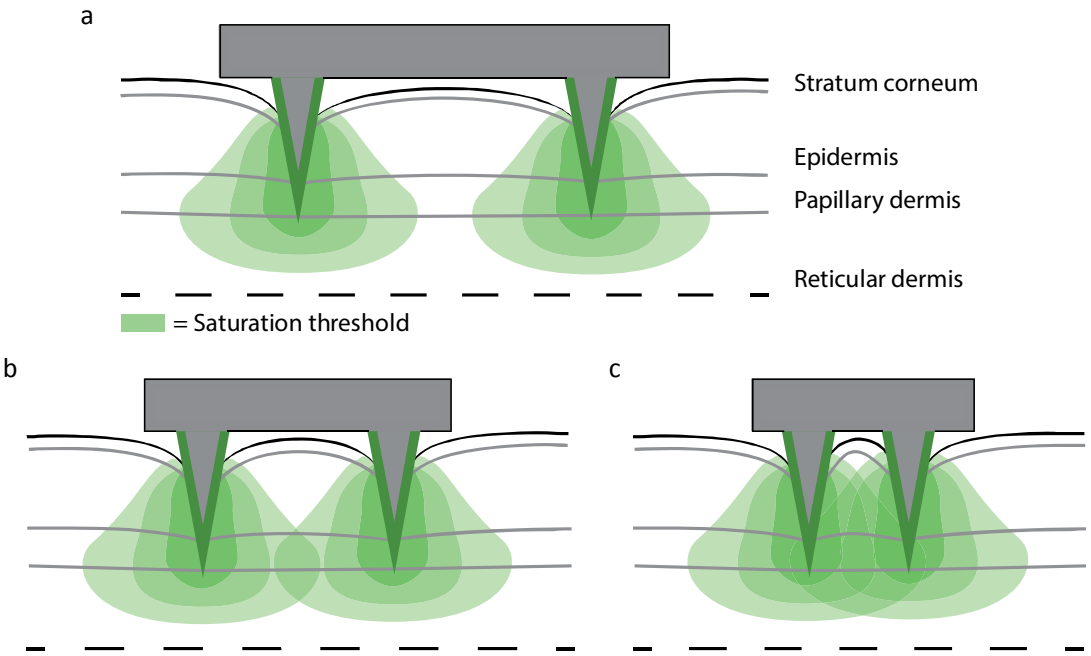


**Figure 9 –** The volume in which cells are activated was dependent on the spacing between microneedles, as visualized in these two-dimensional drawings of a large (a), optimal (b), and small (c) distance between microneedles. The area in which the saturation exceeds the saturation threshold is largest for the optimal spacing.